Heliyon 10 (2024) e34360

Contents lists available at ScienceDirect

Heliyon

journal homepage: www.cell.com/heliyon

ELANE is a promising prognostic biomarker that mediates pyroptosis in gastric cancer

Ming Cui [a,1], Xiaowu Wang [b,1], Haiyan Qiao [c], Shixi Wu [a,**], Bingbing Shang [a,*]

[a] *The Second Hospital of Dalian Medical University, Dalian, Liaoning province, China*
[b] *The Third Affiliated Hospital of Wenzhou Medical University, Ruian, Zhejiang Province, China*
[c] *Laboratory Animal Center, Dalian Medical University, Dalian, Liaoning Province, China*

ARTICLE INFO

Keywords:
ELANE
Gastric cancer
Pyroptosis
Immune cells
Clinical prognosis

ABSTRACT

Background: Gastric cancer (GC) is a typical malignant tumor and the main cause of cancer-related deaths. Its pathogenesis involves multiple steps, including pyroptosis, although these steps are still uncertain. Pyroptosis, also known as gasdermin-mediated programmed necrosis, participates in various pathological processes in tumors, including GC. *ELANE*, which encodes neutrophil elastase, is closely associated with GC. Additionally, *ELANE* has been implicated in GC cell pyroptosis, but this has not been confirmed. Therefore, investigating the link between *ELANE* and pyroptosis in GC is warranted. This research uses bioinformatics and experiments to examine the relationship between *ELANE*, pyroptosis, and GC prognosis.

Methods: The GEO and TCGA databases, along with pyroptosis-related genes, were applied to identify pyroptosis-related differentially expressed genes (DEGs). *ELANE* was selected via primary screening. Using the median expression level of *ELANE* as the threshold, pyroptosis-related DEGs were divided into low- and high-*ELANE* groups. Based on the DEGs in these two groups, GO, KEGG and GSEA analyses were conducted to elucidate the mechanisms of *ELANE* in GC. Furthermore, we plotted ROC and Kaplan–Meier curves to analyze the clinical and pathological features of *ELANE* expression. The Nomograms tool was applied to calculate the predictive value of *ELANE* for the clinical outcomes of GC cases. Immunohistochemical analysis was performed to detect the level of *ELANE* in GC tissues and to validate whether *ELANE* was involved in pyroptosis in GC cells through cell experiments. Finally, the immune infiltration of *ELANE* was investigated, and interaction networks (proteins-*ELANE*, microRNA-*ELANE*, and small-molecule drug-*ELANE*) were constructed.

Abbreviations: GC, Gastric Cancer; DEGs, Differentially Expressed Genes; TCGA, The Cancer Genome Atlas; GEO, Gene Expression Omnibus; STRING, Search Tool for the Retrieval of Interacting Genes/Proteins; ENCODE, Encyclopedia of DNA Elements; GO, Gene Ontology; KEGG, Kyoto Encyclopedia of Genes and Genomes; GSEA, Gene Set Enrichment Analysis; TIMER, Tumor Immune Estimation Resource; PPI, Protein-Protein Interaction; CEA, carcinoembryonic antigen; CA, carbohydrate antigen; OS, overall survival; DFS, disease-free survival; PFI, progression-free interval; ROC, Receiver Operating Characteristic; AUC, area under the curve; CI, confidence interval; FDR, false discovery rate; IHC, Immunohistochemistry; NE, Neutrophil Elastase; GSDMD, Gasdermin D; GSDME, Gasdermin E; GSDMC, Gasdermin C; PRG, pyroptosis-related gene; NF-κB, Nuclear Factor Kappa B; miRNA, microRNA; TF, Transcription Factor; FBS, Fetal Bovine Serum; LPS, Lipopolysaccharide; RT-qPCR, Reverse Transcription-quantitative Polymerase Chain Reaction; TMA, The tissue microarray; ADO, purine nucleoside adenosine; PI3K, Phosphoinositide 3-Kinase; MAPK, mitogen-activated protein kinase.

* Corresponding author.
** Corresponding author.
E-mail addresses: wushixidoctor@126.com (S. Wu), shangbingbing@dmu.edu.cn (B. Shang).
[1] The authors contributed equally: Ming Cui, Xiaowu Wang.

https://doi.org/10.1016/j.heliyon.2024.e34360
Received 28 April 2024; Received in revised form 8 July 2024; Accepted 8 July 2024
Available online 15 July 2024

Results: We aimed to investigate the expression of the *ELANE* gene in GC and study the relationship among *ELANE*, pyroptosis, and the prognosis of patients with GC. Differential expression analysis of gene-expression datasets from TCGA-STAD and GSE49051 revealed that the expression of the *ELANE* gene was significantly up-regulated in GC. Using STRING network analysis, we identified multiple proteins involved in the occurrence and development of GC, including interactions between *ELANE* and GSDMC, a member of the gasdermin protein family. Survival analysis showed that *ELANE* expression levels significantly affected overall survival (OS), disease-free survival (DFS), and progression-free survival (PFS) in patients with GC. Additionally, ROC analysis demonstrated that *ELANE* was effective in distinguishing GC patients from normal controls (AUC = 0.812). Immunohistochemical analysis showed that *ELANE* was highly expressed in gastric cancer tissues and was closely related to age, tumor grade, and stage. The cell experiments further confirmed that the high expression of *ELANE* in gastric cancer cells was associated with pyroptosis. Comprehensive analysis indicated that *ELANE* could be used as a potential prognostic marker for GC and plays an important role in pyroptosis.
Conclusion: High *ELANE* expression is related to poor survival and prognosis of patients with GC. It participates in pyroptosis and immune infiltration in GC. Therefore, *ELANE* is a promising prognostic biomarker for pyroptosis in GC.

1. Introduction

Gastric cancer (GC) is the leading cause of cancer-related deaths and is a highly prevalent form of malignant tumor in the digestive system [1,2]. Approximately 1 million new patients with GC are diagnosed worldwide annually, and cases with advanced GC have a 5-year survival rate of 18–29 % [3]. This imposes pressure on the global economy and public health. Despite significant advances in GC therapy, the prognosis for advanced GC is still discouraging due to the complex etiology of the disease and limited therapy options. Typically, in the diagnosis of GC, the tumor–lymph node–metastasis (TNM) classification is a standard adopted to assess the risk of GC in clinical settings. Additionally, carcinoembryonic antigen (CEA) and carbohydrate antigen (CA) 19–9, as serum tumor markers, are widely used to assess malignancy and recurrence and predict the therapeutic effect of GC [4,5]. However, CEA and CA19-9 values do not necessarily reflect clinical features, especially their lack of sensitivity and specificity for the early recognition of GC, its recurrence, and prognosis [6]. To date, diverse prognostic biomarkers have been discovered through experimental and metagenomic screening, especially with the rapid development of recent advancements in bioinformatics technology. Therefore, identifying novel molecular biomarkers for forecasting the diagnosis and prognosis of GC is crucial.

Pyroptosis [7], also known as gasdermin-mediated programmed necrosis, participates in multiple pathological processes in tumors, including GC. When Gasdermin D (GSDMD) was cleaved by inflammatory caspase, and Gasdermin E (GSEME) was cleaved by apoptotic caspase, cell death by pyroptosis resulted in the cell became swelling, and the plasma membrane ruptured; ultimately, the intracellular content released into the microenvironment. Recent studies suggest that pyroptosis is important in promoting or inhibiting tumor development [8–10]. Zhou et al. revealed that statins could induce ARID1A inactivated cells pyroptosis in clear cell ovarian carcinoma via the inhibition of the mevalonate pathway [11]. With the advancement of bioinformatics technology and the expansion of genome databases, a pyroptosis-related gene (PRG) signature has been utilized for cancer detection and/or prognosis prediction [12–14]. Therefore, many scholars have explored new PRGs for GC, focusing on building a clinical prediction model of GC. However, the specific regulation mechanisms of pyroptosis in GC are still unclear, especially looking for new variants of PRGs in GC. This study used bioinformatic data to screen a PRG——*ELANE*.

ELANE, which encodes neutrophil elastase, is located on chromosome 19 [15]. It is one of six elastase genes found in humans. It encodes a preprotein that is converted into an active protease capable of hydrolyzing proteins in specialized neutrophil lysosomes and proteins in the extracellular matrix to perform biological functions. Previous studies have linked *ELANE* mutations to illnesses such as periodic neutropenia, severe congenital neutropenia [16], and acute pancreatitis [17]. In the field of tumor research, the *ELANE* gene promotes the formation of lung tumors by degrading insulin receptor substrate-1 [18,19]. *ELANE* is associated with the prognosis of renal clear cell renal carcinoma [20] and endometrial carcinoma [21]. There have been two related studies in the field of GC. Among these, one study focused on the association of *ELANE* level and GC prognosis as well as immune infiltration [22], while another study discovered that *ELANE* was implicated in GC cell pyroptosis [23]. However, whether *ELANE* plays a role in cell pyroptosis in GC as a promoter or suppressor, thus affecting the GC outcome, remains unclear.

This research aimed to investigate the GO, KEGG, GSEA, Friends analysis, and prognostic performance of *ELANE* signatures in GC using bioinformatics. Moreover, we also explored the relationship between *ELANE* and immune cell infiltration. Lastly, interaction networks (proteins-*ELANE*, miRNA-*ELANE*, TF-*ELANE,* and small-molecule drugs-*ELANE*) were built to predict the transcription, translation, expression, gene function, and target drug of *ELANE*. Additionally, we verified the expression levels of *ELANE* using the tissue microarray of GC. Moreover, the relationship between *ELANE* and GC pyroptosis was verified, providing a basis for how *ELANE* affects GC via pyroptosis. Furthermore, we studied the underlying mechanism using bioinformatics. The above findings may provide novel insights into the early diagnosis, therapeutic target, and prognosis evaluation of GC.

2. Materials and methods

2.1. Acquisition of data and differentially expressed genes (DEGs)

GSE49501 from the GEO (Gene Expression Omnibus) database was downloaded using the "GEOquery" [24] package, which comprises six samples, three GC tissues, and three normal tissues. Additionally, the "TCGAbiolinks" [25] software was applied to download the TCGA-STAD database. Simultaneously, clinical data of the corresponding patients were acquired, including age, sex, living status, follow-up time, tumor–lymph node–metastasis stage, and pathological stage. The cases were divided into 373 GC and 32 healthy individuals. The "Limma" [26]package was employed for the GEO dataset to identify the DEGs. Genes with logFC >0.58 (or logFC <–0.58) and adjusted $p < 0.05$ were classified as up-regulated (or down-regulated) DEGs. Similarly, for the TCGA dataset, the "DESeq2" [27] package was used to select the DEGs, and genes with logFC >1(or logFC <–1) and adjusted $p < 0.05$ were considered up-regulated (or down-regulated) DEGs. Finally, the "ComplexHeatmap" [28] package was utilized to visualize the DEGs.

Furthermore, we intersected the DEGs (from both datasets) with genes related to pyroptosis to identify the key genes associated with pyroptosis in GC. The median level of *ELANE* was used as the threshold, and the GC group (375 patients) was categorized into two subgroups: the high-*ELANE* group and the low-*ELANE* group (188 and 187 cases, respectively) (see Supplementary Table S1). Based on the "DESeq2" software, DEGs were obtained for further analysis.

2.2. Functional enrichment analysis of the DEGs

The R package "clusterProfiler" [29] was used to perform GO functional annotation analysis and KEGG analysis on DEGs.

2.3. Gene set enrichment analysis (GSEA)

GSEA [30] is applied to assess the distribution trend of genes in a predefined gene set in the gene table to judge its influence on phenotype. For this study, the "c2.all.v7.4. symbols" gene set from the Molecular Signatures Database was obtained, and GSEA analysis was performed using the "clusterprofiler" R software package. A false discovery rate (FDR) < 0.25 was considered as significantly enriched.

2.4. Friends analysis

The Friends analysis method was applied to identify the key genes. It is mainly applied to determine the functional association between a gene and other genes in a pathway. We assumed that if a gene interacted with other genes in the pathway, it could be regarded as a key gene. To analyze the key gene, the R package "GOSemSim" [31] was used to clarify the functional correlation between the DEGs in two *ELANE*-expressed GC groups. The top 10 genes with the strongest functional correlations among the differentially upregulated or downregulated genes were regarded as key genes.

2.5. Construction of ELANE interaction networks

The Search Tool for the Retrieval of Interacting Genes/Proteins (STRING) database [32] was applied to construct the PPI network for key DEGs related to high and low expression of *ELANE* in GC. We obtained the miRNA-gene interactive network from the miRTarBase v8.0 database via the NetworkAnalyst platform [33] and utilized the chromatin immunoprecipitation data from the Encyclopedia of DNA Elements (ENCODE) database [34] to construct the miRNA-key gene and transcription factor-key gene networks for key genes. The output results from the NetworkAnalyst database [33] were visualized using Cytoscape software (https://cytoscape.org/). STITCH [35] was used to construct a small-molecule drug-target gene interaction network.

2.6. ELANE gene analysis

We analyzed *ELANE*'s ability to distinguish normal tissues from GC, drew ROC curves for each gene based on the "pROC" [36] software, and determined the area under the curve (AUC). Using the complete clinical data of patients with GC, we compared the differences in overall survival (OS), disease-free survival (DFS), and progression-free interval (PFI) between patients with GC and those with different *ELANE* levels across various clinical subgroups.

ELANE, with an AUC >0.6 and prognostic significance, was selected as the key gene related to pyroptosis in GC. Simultaneously, we analyzed the association between *ELANE* levels and different pathological factors. Time-dependent ROC can utilize additional information on each individual's onset time to form ROC curves at multiple actual points and compare the predictive abilities of different factors. The "timeROC" [37] package was used to predict the survival outcome of cases for 1, 3, and 5 years. A univariate Cox analysis was performed to clarify the association between different pathological features and the OS rate of the cases, and clinicopathological features ($p < 0.1$) were selected for multivariate Cox analysis. Clinicopathological features ($p < 0.05$) were considered independent factors affecting the prognosis of patients with GC; the corresponding factors were included in the model. A nomogram was applied to predict the survival of cases at different years. We evaluated whether the predicted values of the model were consistent with the probability of the outcome event by drawing a calibration plot of the model.

2.7. Immune infiltration analysis

The "CIBERSORT" method was applied to analyze the immune infiltration of the sample and identify immune cells that were differentially enriched in the data of two *ELANE* level groups [38]. The Tumor Immune Estimation Resource (TIMER) database uses a deconvolution approach to determine the abundance of such cells based on gene expression information. This study detected the expression level of *ELANE* in GC during research and conducted correlation analysis to clarify its relationship with immune infiltrating cells, in order to determine the role of *ELANE* in the pathological process of GC.

2.8. Immunohistochemical (IHC) verification of ELANE expression level in gastric tumor tissues of patients with GC

The tissue microarray (TMA) of gastric cancer tissues and adjacent normal mucosa tissues (HStm-Ade060PG-01) was purchased from Shanghai Outdo Biotech Company (Shanghai, China). We performed an immunohistochemistry analysis on TMA. The steps of IHC have been previously described in detail [39]. Subsequently, we judged the result based on the following conditions: 1) staining intensity score: 0 (negative), 0.5 (0.5 +), 1 (1 +), 2 (2 +), and 3 (3 +); 2) positive staining rate score: 0–100 %; 3) total score: "staining

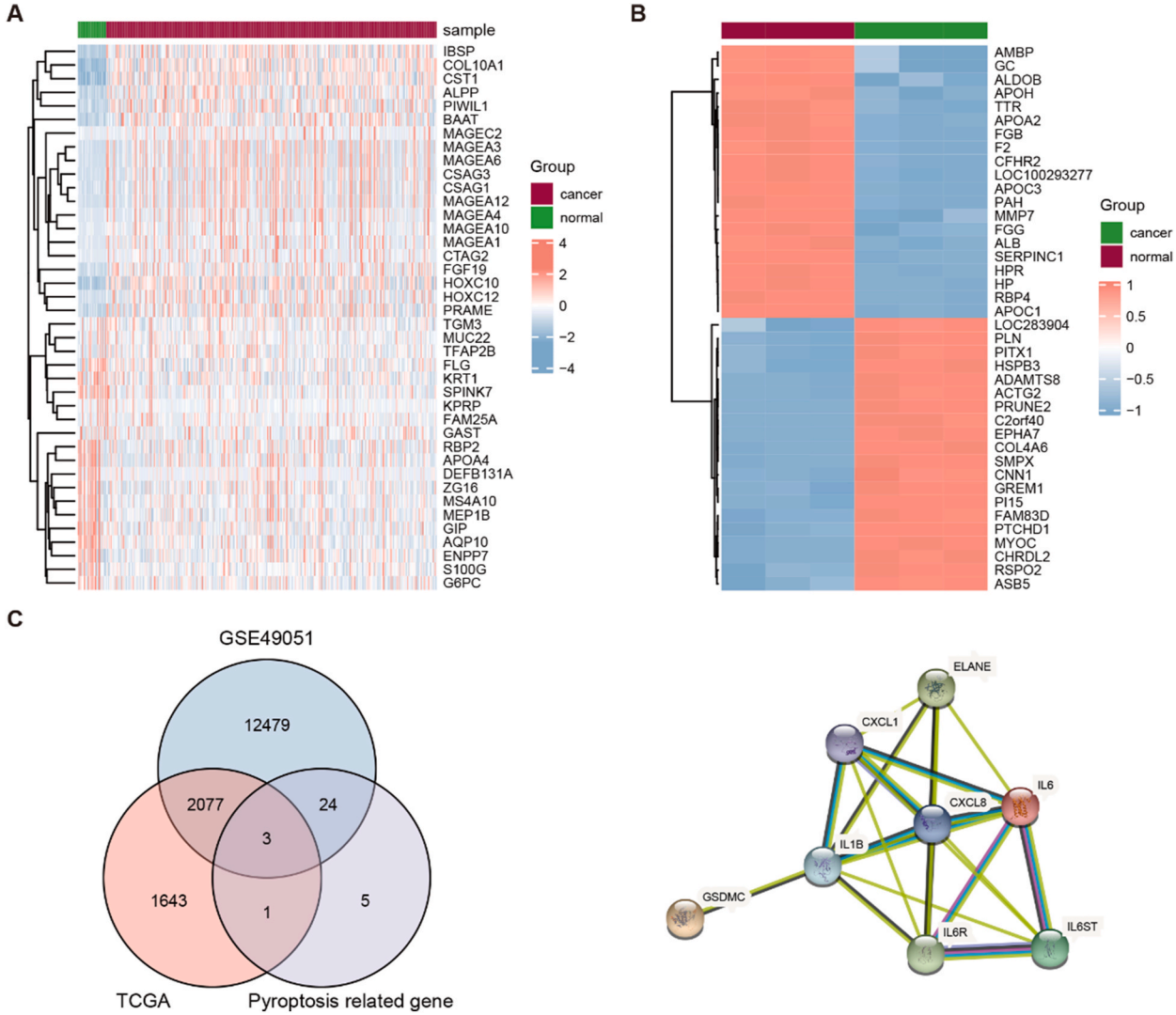

Fig. 1. Differential expression of key genes related to pyroptosis in GC. (A–B): DEGs in GC from the TCGA-STAD dataset and the GSE49051 dataset. The abscissa of A and B represents the patient ID, while the ordinate represents their respective DEGs. Red indicates high gene expression, blue indicates low gene expression, purple annotation bars represent normal tissues, and green annotation bars represent tumor tissues. These annotation bars show the DEGs in these datasets. (C): A Venn diagram of three databases. The pink circle represents the DEGs in the TCGA-STAD dataset, the blue circle represents the DEGs in the GSE49051 dataset, and the purple circle represents the genes related to pyroptosis. The key genes related to pyroptosis are obtained by intersection. (D): PPI of differentially expressed key genes related to pyroptosis in GC.

intensity score" multiply by "positive rate" (0–300 %); and 4) *ELANE* expression level analysis: 160 % of the total score was designated the low-level group, while >160 % was the high-level group.

2.9. Cell experiments to verify ELANE expression level and its relationship with pyroptosis in GC cells

Cell sources: GES and AGS cells were purchased from the China Cell Bank (Beijing, China) through reagent suppliers. The cell culture conditions are as follows: constant-temperature cell incubator with 5 % CO_2 at 37 °C, medium with RPMI 1640 (Gibco, Thermo Fisher Scientific, Waltham MA, USA) +10 % fetal bovine serum (Gibco, Thermo Fisher Scientific) +1 % double antibiotics (penicillin and streptomycin) (Gibco, Thermo Fisher Scientific) for GES cells, and AGS-specific medium (Punuosai Life Science and Technology Co., Ltd, China) for AGS cells. According to the previous work, we first treated the cells with 500 μg/mL lipopolysaccharide (LPS) (Sigma Aldrich, Burlington, MA, USA) for 4 h and then treated via them with 5 mM ATP (Sigma Aldrich) for 36 h to establish a cell pyroptosis model. Subsequently, the experimental groups were designated as GES, GES + LPS + ATP, AGS, and AGS + LPS + ATP. Finally, the cells were collected for RT-qPCR experiments, western blotting, and electron microscopy experiments, as described in previous research [40].

2.10. Statistical analysis

All data analyses were conducted on R (version 4.0.2; R Foundation for Statistical Computing, Vienna, Austria). Since there are significant prior differences between the groups and differences in specific contrasts need to be identified, we opted for a pairwise comparison. For normally distributed measurement data, we applied the *t*-test when comparing the differences in results between groups. For non-normally distributed measurement data, we used the *U* test is used for difference analysis (i.e., the Wilcoxon rank-sum test).

3. Results

3.1. Pyroptosis-related DEGs in GC

To obtain DEGs in two types of tissues, we conducted a multi-data differential gene analysis. As shown in Fig. 1A–C, 3768 DEGs were obtained from TCGA-STAD data, containing 1713 upregulated and 2055 downregulated genes (Fig. 1A). Simultaneously, 14,664 DEGs were obtained in GSE49051, containing 1144 upregulated genes and 13520 downregulated genes (Fig. 1B). These two gene sets interacted with the representative genes involved in pyroptosis, and we identified three key genes, including *ELANE*. Additionally, STRING web analytics were used to identify the proteins (*ELANE*, CXCL1, CXCL8, IL1B, IL-6ST, IL-6R, IL-6, and Gasdermin C(GSDMC)) that may be involved in the occurrence and development of GC. Moreover, other studies have shown that *ELANE* interacts with GSDMC, a key protein involved in pyroptosis (Fig. 1D).

Using the relevant clinical data of cases with GC, we grouped patients with GC according to the median level of these genes and compared the OS differences between different groups. According to the analysis result, only the *ELANE* gene level significantly affected OS (Fig. 2A), DFS (Fig. 2B), and PFI (Fig. 2C) of patients with GC, indicating that the pyroptosis-related gene *ELANE* may play an important role in the GC prognosis. Additionally, ROC analysis of DEGs related to GC pyroptosis of *ELANE* showed that the AUC of *ELANE* in the TCGA dataset (Fig. 2D) was 0.812 (0.736–0.887), indicating that *ELANE* had a good ability to distinguish GC from the normal control group. In summary, the above results indicated that *ELANE* is closely related to the prognosis of GC and pyroptosis.

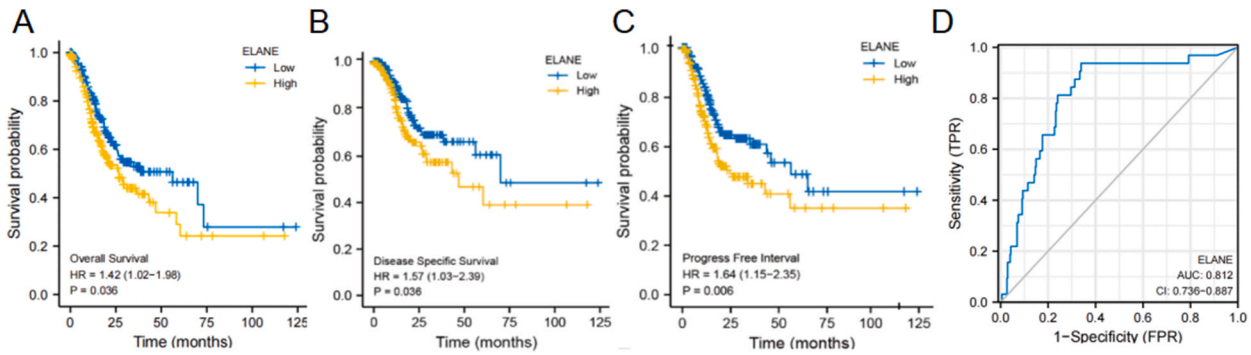

Fig. 2. Gastric cancer survival prognosis analysis of the *ELANE* gene in TCGA-STAD data. (A–C): Survival analysis of *ELANE* gene expression level, grouped by the median of *ELANE* gene expression level. Blue lines represent the low-*ELANE* gene expression group, and yellow lines represent the high-*ELANE* gene expression group. The horizontal axis is survival time, and the vertical axis is survival probability. (D): A ROC curve, where the x-axis is 1-specificity, and the y-axis is sensitivity. The AUC and the 95 % confidence interval (CI) are noted in the lower right corner.

3.2. Differential expression analysis of low/high expression groups of ELANE in patients with GC

Considering that *ELANE* is closely related to the prognosis of GC, we separated the 373 patients with GC into a high and low *ELANE* level group (186,187 patients) (Supplementary Table S1), using the median level of *ELANE* as the cut-off value. The DEGs were identified using the "DESeq2" package. We obtained 2280 DEGs, of which 2239 were upregulated genes and 41 were downregulated genes, as shown in a volcano plot (Fig. 3A). The top 20 genes were shown in a heatmap (Fig. 3B). The similar expression patterns of multiple genes suggest that they may form functional complexes acting in concert. Subsequently, we analyzed the heatmap of the top 10 genes with strong correlations with *ELANE* expression (Fig. 3C), and it was found that *ELANE* and *TSPAN6* were most evidently associated.

3.3. ELANE gene and clinical pathological characteristic

Subsequently, this study analyzed the association between the pathological features of cases with GC and *ELANE* expression. *ELANE* expression was higher in older GC cases (Fig. 4A), histologically graded G3 stage (Fig. 4B), and T2 stage (Fig. 4C). In the subgroup analysis of different clinical features, we found that in patients with GC aged <65 years, histological grade G3 and T3–4, the expression level of *ELANE* had an impact on OS (Fig. 4D–F). Low *ELANE* level was related to a better prognosis in GC cases. We evaluated the predictive efficacy of *ELANE* expression for OS (Fig. 4G), DFS (Fig. 4H), and PFI (Fig. 4I) using time-dependent ROC curves. According to the ROC analysis result, *ELANE* can effectively predict the 5-year DFS, with an AUC of 0.7. Next, we conducted univariate Cox analysis based on *ELANE* levels and clinicopathological features, and found that age, grade, stage, and expression of *ELANE* were unfavorable factors for patient prognosis (Fig. 5A; Supplementary Table S2). We included factors with $p < 0.1$ and conducted multivariate Cox analysis, the results revealed that age, M stage, and expression of *ELANE* can be seen as the independent risk factors for the prognosis of GC cases (Fig. 5B; Supplementary Table S2). Subsequently, a nomogram (Fig. 5C) was constructed using age, M stage, and *ELANE* gene level to predict the survival rates of GC cases. Based on the calibration curve, it can be indicated that the above model can effectively predict the 1- and 3-year survival rates of GC cases (Fig. 5D).

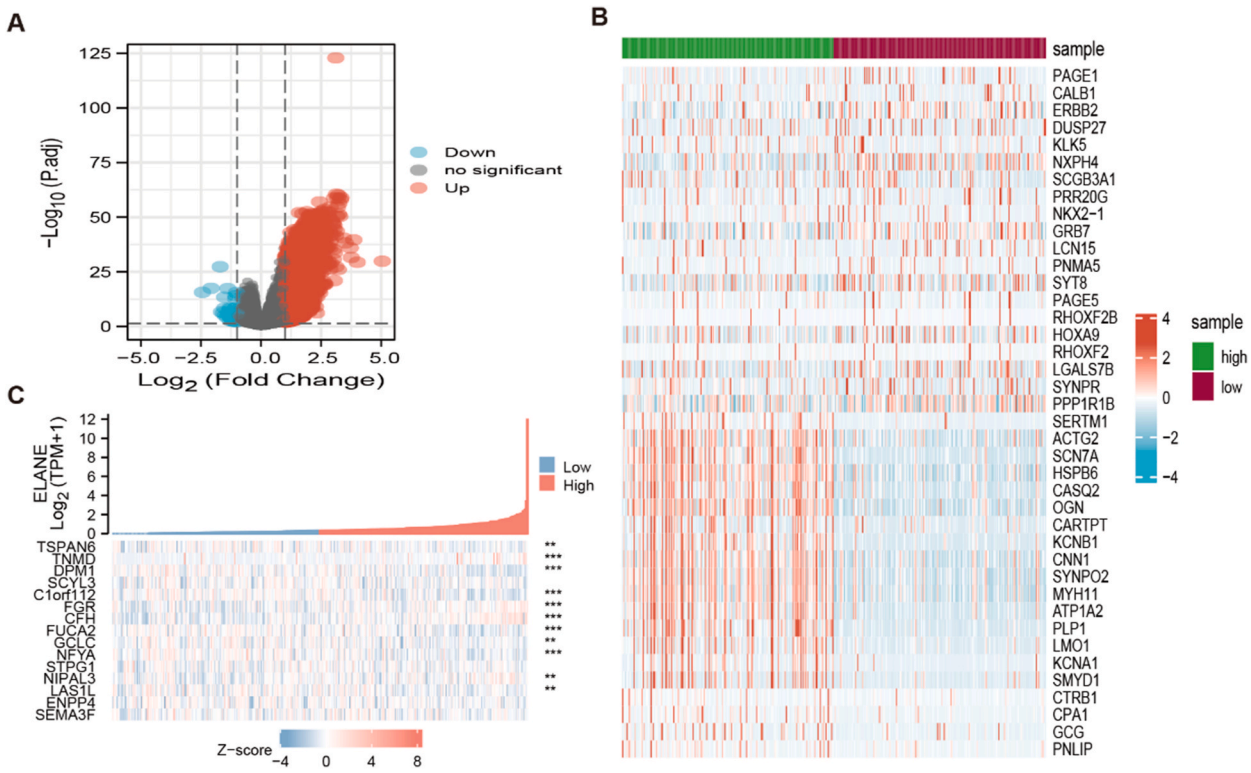

Fig. 3. Taking the median expression level of *ELANE* as the threshold, the GC group was divided into two subgroups: the high-*ELANE* group and the low-*ELANE* group, and then differential expression was analyzed. (A): A volcano plot of differential expression, where the x-axis represents log2-FoldChange, and the y-axis is -log10(Adjusted *P*-value). Red nodes indicate up-regulated DEGs, blue nodes indicate down-regulated DEGs and gray nodes represent genes that are not significantly differentially expressed. (B): A heatmap of differential expression, where the x-axis represents patient IDs, and the y-axis is their respective DEGs. Red indicates high gene expression, blue indicates low gene expression, the purple annotation bar represents the high-*ELANE* group, and the green annotation bar represents the low-*ELANE* group. (C): A thermogram of the expression of *ELANE*-related genes. Red indicates high gene expression, blue indicates low gene expression, and the x-axis represents different GC individuals.

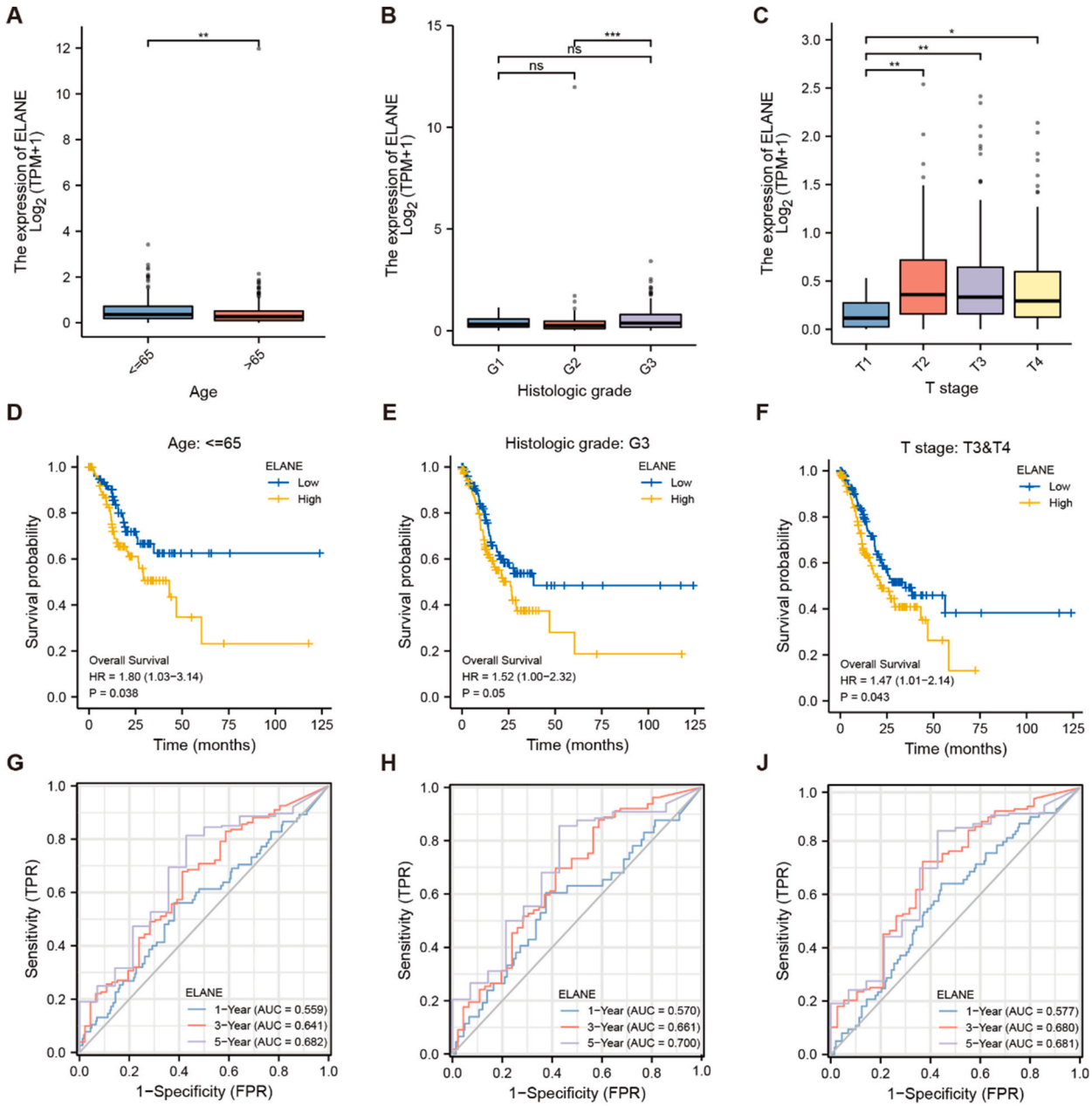

Fig. 4. *ELANE* and Clinicopathological Features. (A–C): The relationship between the expression level of *ELANE* in patients with GC and the clinicopathological features of patients in the TCGA dataset. The x-axis represents different clinicopathological features, and the y-axis indicates the expression level of the *ELANE* gene. (D–F): Survival analysis of subgroups of patients with GC in the TCGA dataset. Blue lines indicate low expression of *ELANE*, and yellow lines indicate high expression of *ELANE*. The horizontal axis represents survival time, and the vertical axis represents survival probability. (G–J): Time-dependent ROC curve. The x-axis is 1-specificity, and the y-axis is sensitivity. The area under the curve and 95 % confidence interval are also indicated.

3.4. Functional enrichment and friends analysis of DEGs between Low-ELANE and High-ELANE groups in patients with GC

GO and KEGG analyses were conducted to enrich DEGs related to *ELANE* in TCGA-STAD. Up-regulated DEGs related to *ELANE* in GC were mainly enriched in "regulation of membrane potential," "sensory perception of smell," "muscle contraction," and other biological processes. Simultaneously, these genes also enriched cellular components such as "transmembrane transporter complex," "transporter complex," and so on. Also, they enriched "ion channel activity", "passive transmembrane transporter activity," and other molecular functions (Fig. 6A, Supplementary Table S3). KEGG results suggested that up-regulated DEGs were mainly enriched in "neuro Active ligand-receptor interaction," "olfactory transport," "dilated cardiomyopathy," and "hypertrophic cardiomyopathy pathways"

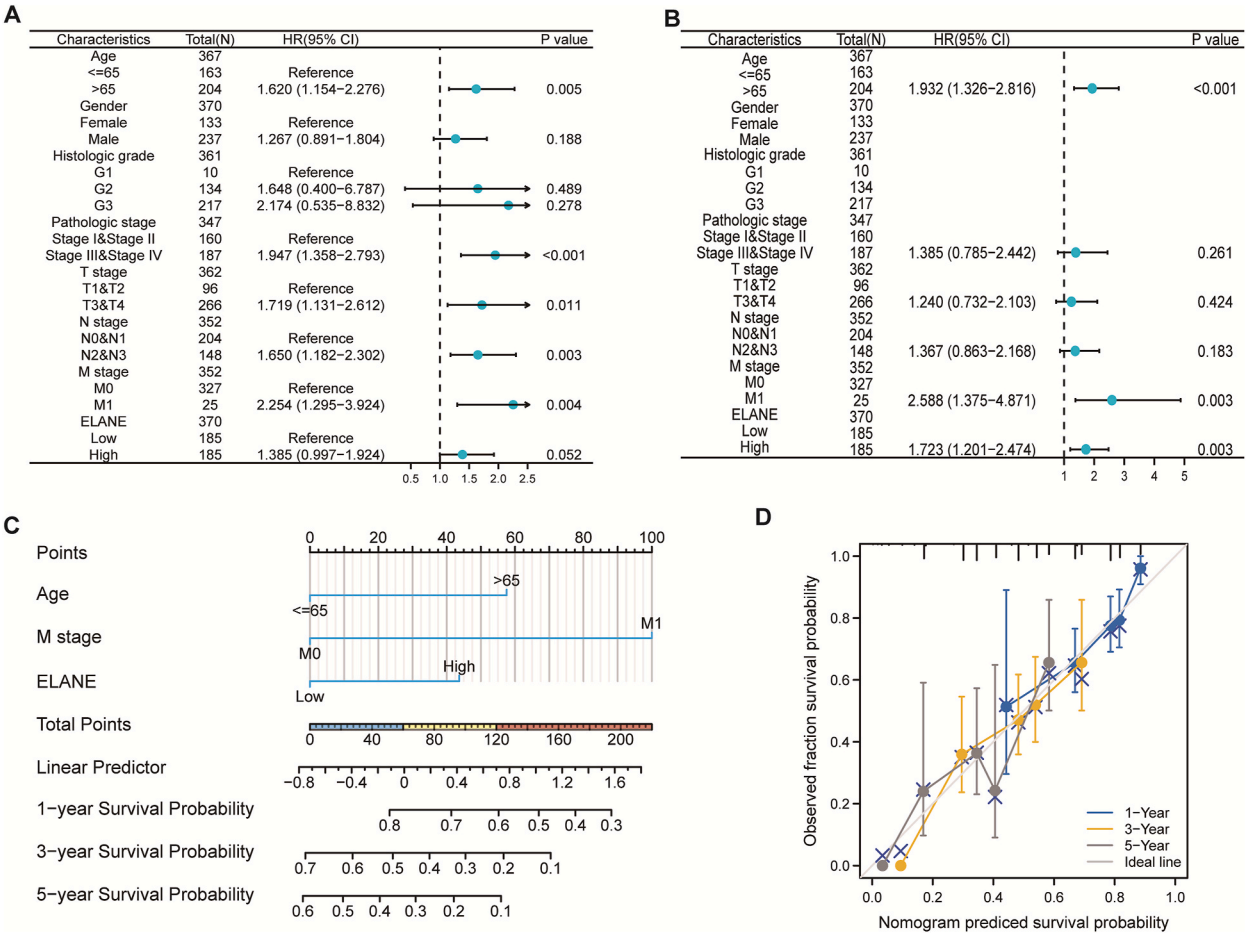

Fig. 5. *ELANE* and Prognosis Model. (A): Forest plot of single-factor Cox analysis. (B): Forest plot of multi-factor Cox analysis. (C): A nomogram predicts the survival of patients at 1 year, 3 years, and 5 years. (D): A calibration chart, with the x-axis indicating the predicted patient survival and the y-axis indicating the actual patient survival.

(Fig. 6A–Supplementary Table S4). Besides, we presented the markedly enriched pathways: HSA04974 ("protein digest and absorption") and HSA04024 ("cAMP signaling pathway") in Fig. 6C and D. In contrast, the down-regulated DEGs related to *ELANE* in GC were mostly enriched in biological processes like "response mediated by antimicrobial peptide," "locomotory behavior," and so on. For the molecular functions, they were enriched in "ferric iron binding," "oxidoreductase activity," and so forth (Fig. 6B). The top 10 key genes of up- and down-regulated DEGs related to *ELANE* in GC were identified via the Friends analysis and visualized using box plots. As shown in Fig. 6E and F, *IGFN1* had the strongest correlation with other upregulated DEGs, and *NKX2-1* had the strongest correlation with other downregulated DEGs; these results indicated that they can be regarded as key factors in the GC pathological process.

3.5. GSEA

To determine the functions of the different gene sets in the two *ELANE* level groups in TCGA-STAD, we performed GSEA. The results (Supplementary Table S5) showed that the gene sets including "KEGG_NEUROACTIVE_LIGAND_RECEPTOR_INTERACTION" (Fig. 7A), "NABA_CORE_MATRISOME" (Fig. 7B), "REACTOME_MUSCLE_CONTRACTION" (Fig. 7C), "NABA_ECM_GLYCOPROTEINS" (Fig. 7D), "WP_GPCRS_CLASS_A_RHODOPSINLIKE" (Fig. 7E), and "REACTOME_ADORA2B_MEDIATED_ANTIINFLAMMATORY_CYTOKINES_PRODUCTION" (Fig. 7F) were mainly enriched in the high-*ELANE* group. The gene sets of "REACTOME_DNA_STRAND_ELONGATION" (Fig. 7G), "REACTOME_ACTIVATION_OF_THE_PRE_REPLICATIVE_COMPLEX" (Fig. 7H) and "REACTOME_EXPORT_OF_VIRAL_RIBONUCLEOPROTEINS_FROM_NUCLEUS" (Fig. 7I) were mainly enriched in the low-*ELANE* group.

3.6. Construction of interaction network

The PPI network was drawn for the top 20 key genes obtained from friend analyses, and the results were visualized using the

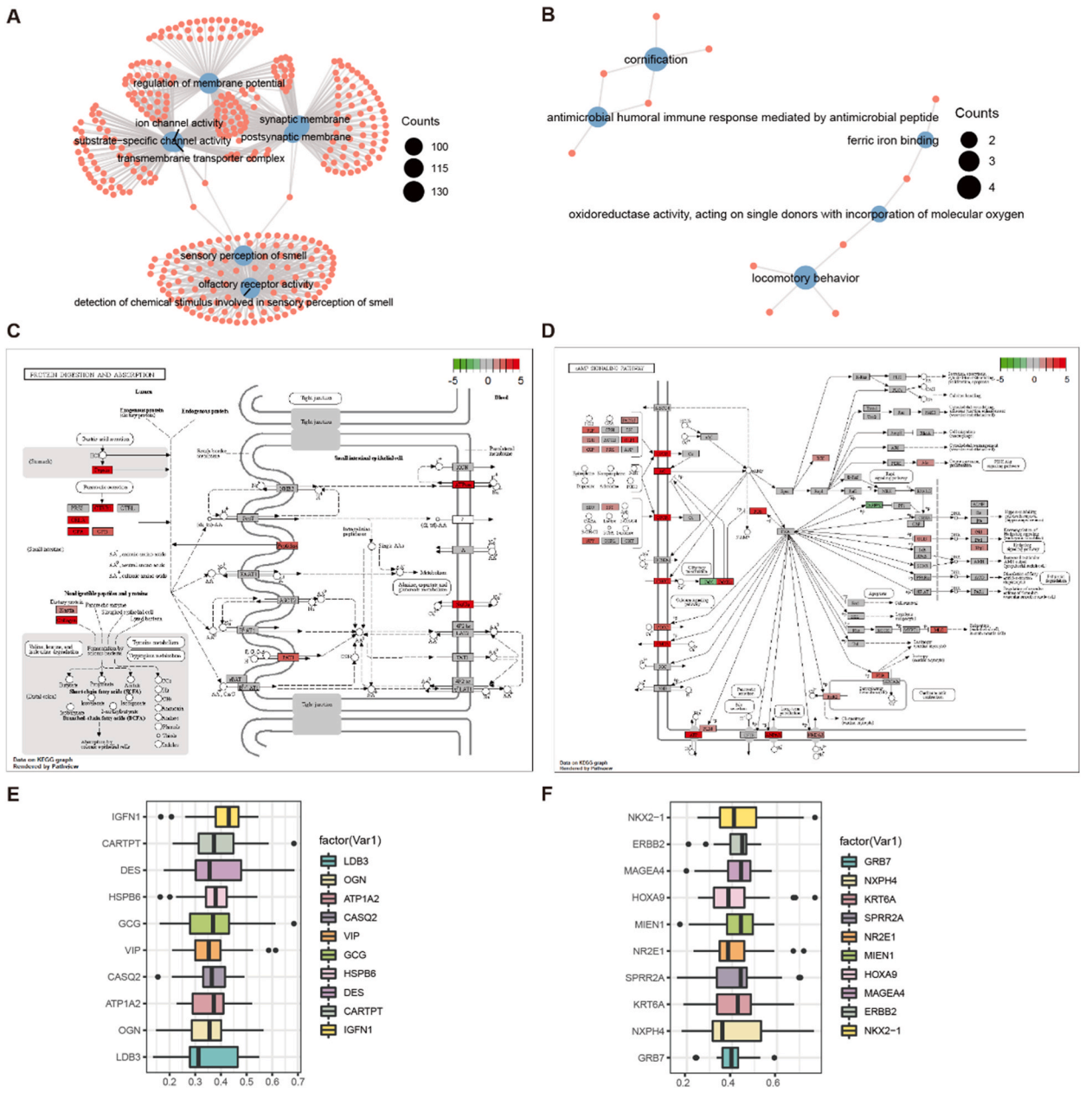

Fig. 6. GO, KEGG enrichment analysis, and Friends analysis. (A–B): GO and KEGG enrichment analysis network diagrams, with red nodes representing different genes and blue nodes representing enriched terms. The size of the blue node indicates the number of genes enriched in the respective pathway. Each functional category shows the top three enriched items. (C–D): Visualization results of the pathway. Each node represents a gene that plays an important role in this pathway, and the color of the node is determined by log2FC; green represents a differentially down-regulated gene, while red represents a differentially up-regulated gene. (E–F): The box plots show the functional similarity analysis between differentially up-regulated genes and differentially down-regulated genes, respectively. The x-axis represents the correlation, and the y-axis represents the gene name.

Cytoscape software. This network comprises 18 nodes and 26 edges (Fig. 8A). Using the Cytoscape plugin MCODE, we identified the modules and displayed them as purple nodes. Another key gene that interacted the most was *ERBB2* (interacting with seven genes), followed by *NKX2-1* (interacting with five genes) (Fig. 8B). MiRNAs and transcription factors play vital roles in gene expression. We constructed the miRNA-*ELANE* and transcription factor (TF)-*ELANE* networks of GC using the NetworkAnalyst database. The miRNA-key gene network comprised four nodes and three edges (Fig. 8C). *ELANE* was regulated by three miRNAs, namely, *hsa-mir-126-3p*, *hsa-mir-146a-5p*, and *hsa-mir-31-5p*. The TF-*ELANE* network consisted of 23 nodes and 22 interaction relationship pairs (Fig. 8D), indicating the degree of interaction between TF and *ELANE* genes in GC. Finally, this study established a network of small-molecule drug-

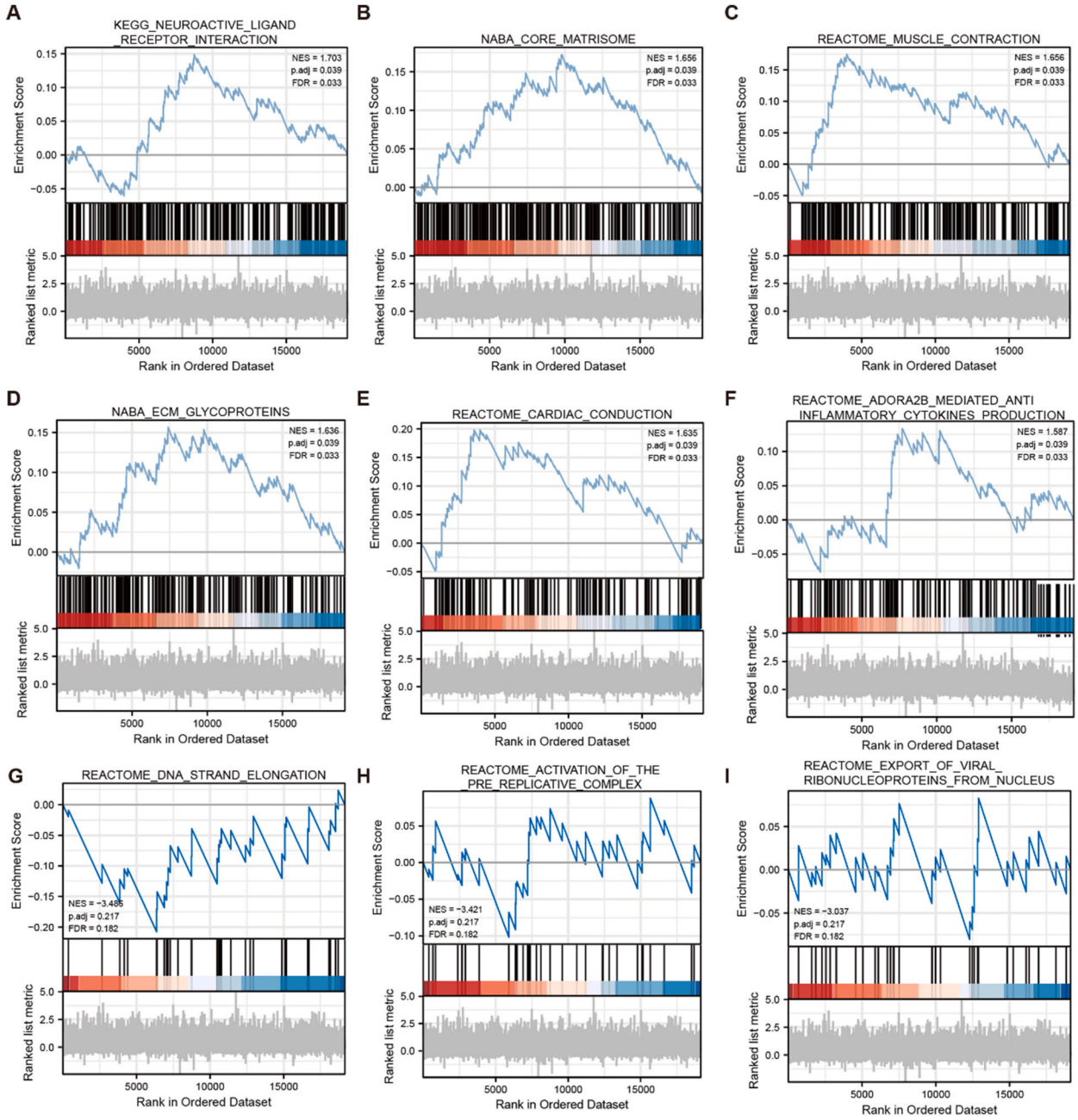

Fig. 7. GSEA analysis. (A–F): The TCGA dataset shows the gene sets enriched in the high-*ELANE* expression group in GC. (G–I): Display of gene sets enriched in the low-*ELANE* expression group in GC from the TCGA dataset.

ELANE gene interactions based on STITCH, and it was found that *ELANE* is a target of 10 small-molecule drugs.

3.7. Immune infiltration analysis

To analyze the difference in immune infiltration levels between the two *ELANE* expression groups in TCGA-STAD, we determined the association between the *ELANE* level and main immune cells using the TIMER database, with a p-value less than 0.05. We found that the *ELANE* level was positively related to B cells, $CD4^+$ T cells, and macrophages and negatively related to tumor purity (Fig. 9A). Additionally, we calculated the infiltration of 22 immune cells using the CIBERSORT method. The proportions of immunocyte infiltration in different samples are shown as stacked bar graphs (Fig. 9B). Using the "wilcox.test" algorithm, 10 immune cells in the TCGA data set showed significant differences between the two *ELANE* groups (Fig. 9C). These included naïve B cells, memory B cells, $CD4^+$

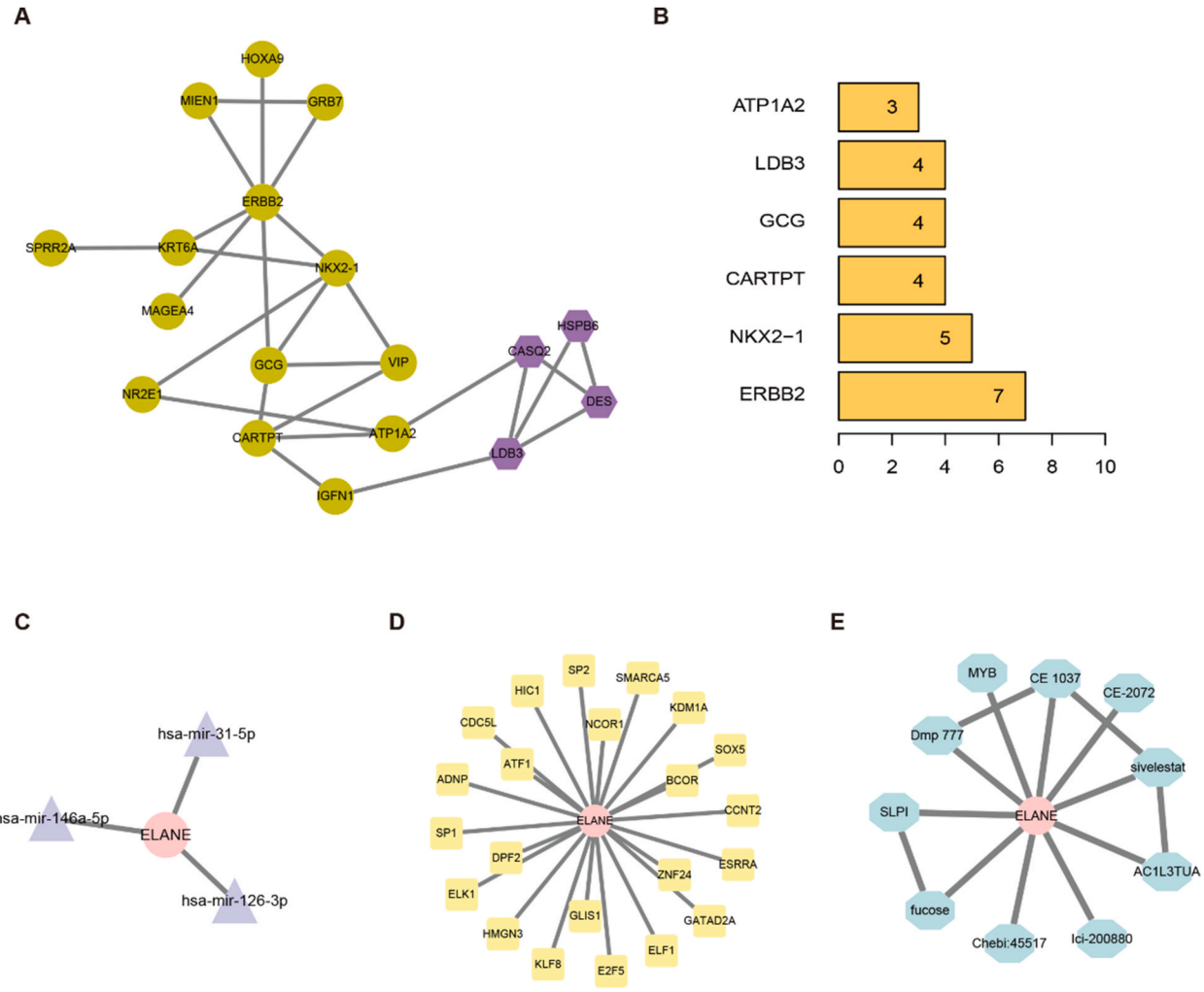

Fig. 8. Construction of interaction network. (A): PPI networks were constructed using the top 10 up-regulated and down-regulated DEGs as the centers in the Friends analysis. (B): A bar chart showing the number of interactions between the first six important nodes and other genes in the protein interaction network. The abscissa represents the gene, and the ordinate represents the number of interaction pairs between the gene and other genes. (C): mRNA-*ELANE* network. Pink round nodes represent *ELANE*, and purple triangular nodes represent interacting miRNAs. (D): TF-*ELANE* network. Pink round nodes represent *ELANE*, and yellow square nodes represent interacting transcription factors. (E): Small molecule drug-*ELANE* network. Pink round nodes represent *ELANE*, and blue nodes represent different small molecule drugs.

memory-activated T cells, activated mast cells, resting NK cells, monocytes, and macrophages.

3.8. IHC verification of ELANE expression level, cell experiments verification of ELANE expression level and its relationship with pyroptosis

IHC analysis of TMA indicated a high *ELANE* level in gastric cancer tissue (Fig. 10A and B). Based on a previous study, we successfully built cell pyroptosis models for normal gastric cells and GC cells, as shown in the electron microscopy experiments (Fig. 10C–E). Subsequently, the experimental groups were designated as GES, GES + LPS + ATP, AGS, and AGS + LPS + ATP. Fig. 10D shows the high *ELANE* level in the GES + LPS + ATP and AGS + LPS + ATP groups and the high *ELANE* level associated with pyroptosis produced in these cells via RT-qPCR. In addition, the AGS + LPS + ATP groups showed higher expression of *ELANE* than the GES + LPS + ATP group, as demonstrated by Western blot and RT-qPCR experiments (Fig. 10D–F, Additional file3).

4. Discussion

Pyroptosis is a type of lytic cell death associated with gasdermin protein. Cells engage in inflammasome assembly, gasdermin cleavage, the generation of proinflammatory cytokines and other cellular materials, and inflammatory cell death in response to external or endogenous signals [41,42]. Many factors, including oncogenic activity and chronic inflammation, regulate tumors. Some scholars have found that chronic exposure to an inflammatory environment is closely associated with a higher cancer risk [43]. The

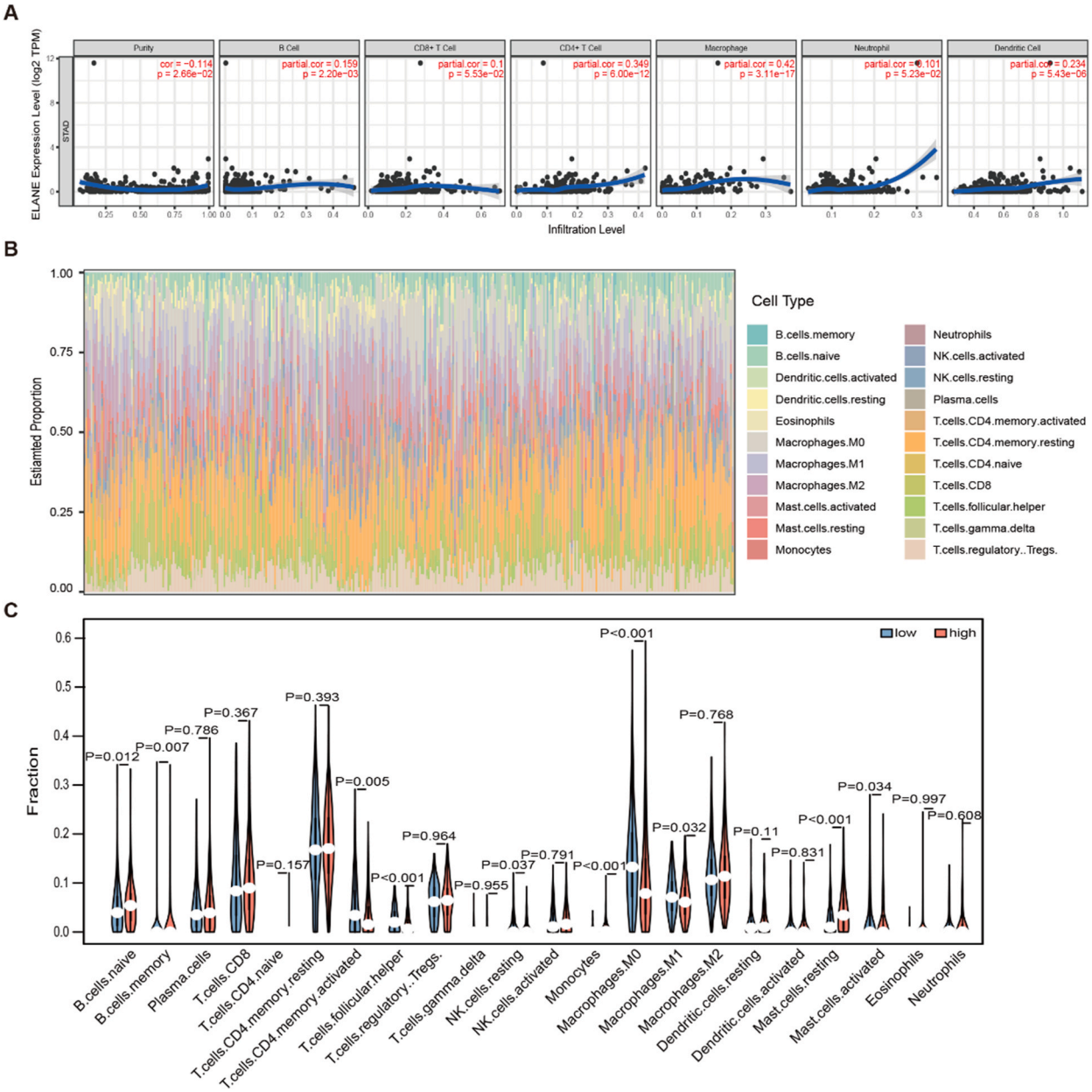

Fig. 9. Immune infiltration analysis. (A): The TIMER database calculates the correlation between *ELANE* expression level and six types of immune cells as well as immune purity. (B): The richness of 22 types of immune cells in patients with gastric cancer. The horizontal axis represents different gastric cancer samples, and the vertical axis represents the abundance of immune cell infiltration. (C): Comparison of immune infiltrating cells between the high-*ELANE* expression group and the low-*ELANE* expression group. Green represents the low-*ELANE* expression group, and red represents the high-*ELANE* expression group, the horizontal axis represents 22 types of immune cells, and the vertical axis represents the infiltration abundance of immune cells.

specific mechanism may be that release of IL-1 and IL-6 [44,45] induced by pyroptosis can increase the infiltration level, thereby enhancing the risk of tumor occurrence and proliferation [46]. These indicate that pyroptosis may play an important role in the clinical diagnosis and treatment of tumors. However, the exact role that pyroptosis plays in the evolution of GC is unclear.

At present, bioinformatics analysis is often used to predict the expression of a gene in tumors and to study various aspects such as clinical prognosis, immune infiltration, PPI, functional pathway and mechanism prediction, and drug-gene prediction. In this study, we performed a series of bioinformatics analyses to explore the target and prognostic biomarkers of GC. Firstly, we conducted differential gene analysis in TCGA and GEO databases through bioinformatics analysis. These two genomes interacted with representative genes of pyroptosis, and we screened *ELANE* as a PRG. *ELANE*, also called neutrophil elastase, is only expressed in mature bone marrow

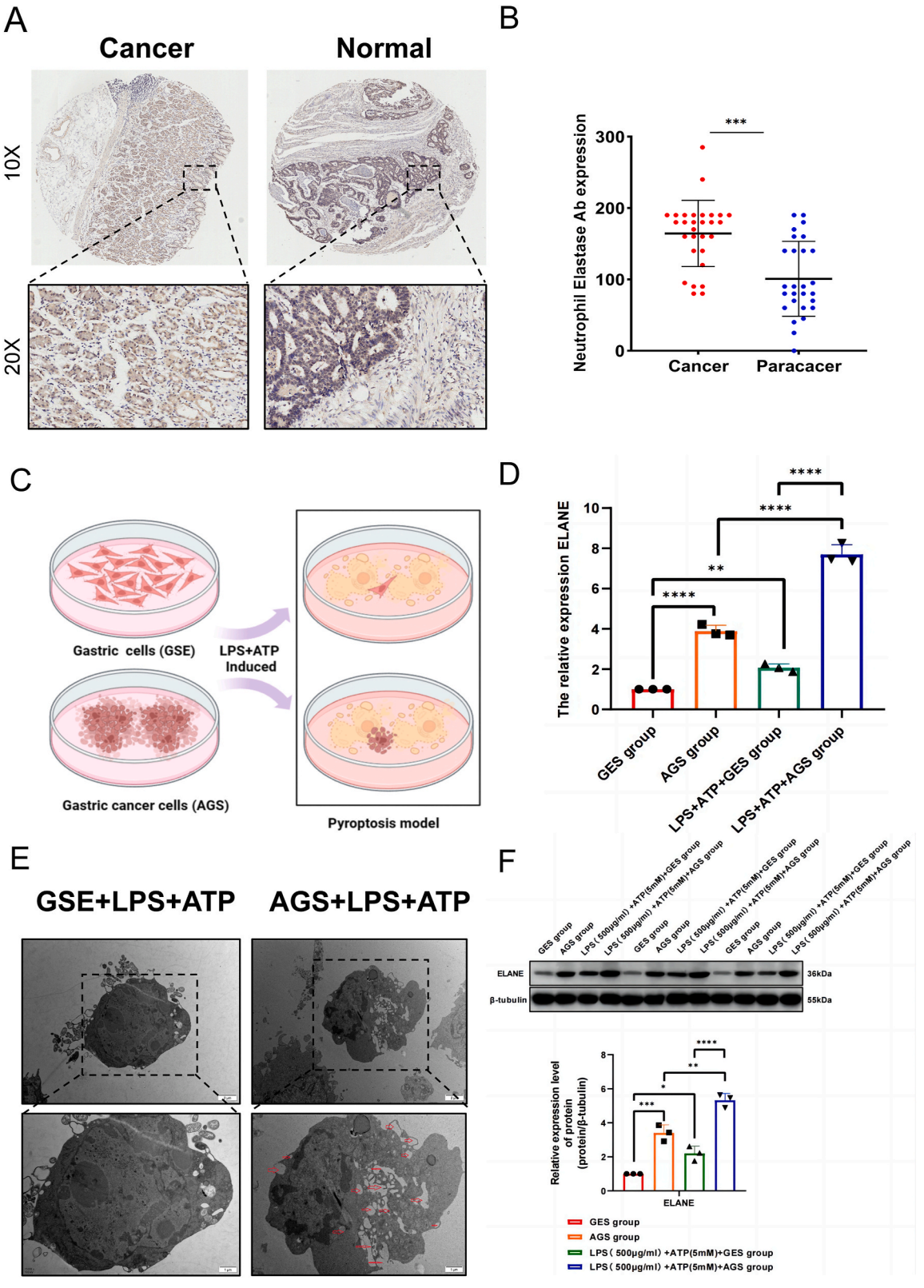

(caption on next page)

Fig. 10. The experiment verified the expression of the *ELANE* gene in GC and its relationship with pyroptosis. (A): Immunohistochemical (IHC) analysis of *ELANE* expression in gastric cancer tissues. Magnification: × 20. (B): The statistics chart of *ELANE* expression in gastric cancer tissues and normal tissues. (C): A schematic diagram of the pyroptosis modeling and grouping of normal gastric cells (GES) and GC cells (AGS). (D): RT-qPCR experiment verified the expression of *ELANE*. (E): Normal gastric cells (GES) and GC cells (AGS) pyroptosis models were observed under an electron microscope. (F): Western Blot experiment verified the expression of *ELANE* in the cell experiment.

mononuclear cells and immature myeloid precursors. Neutrophils release a small amount of *ELANE* under normal conditions; however, neutrophils release a large amount of *ELANE* during infection, which could be involved in tumor development and progression [44]. As an essential part of the neutrophil extracellular traps (NETs) [22], *ELANE* has been recently shown to selectively destroy various cancer cells while causing no harm to neighboring cells. Additionally, *ELANE* can limit tumor growth by inducing apoptosis [45]. However, in acute promyelocytic leukemia, the situation is rather different; *ELANE* could promote leukemia cell growth and inhibit apoptosis by activating the PI3K/AKT signaling pathway [47]. High *ELANE* expression is associated with poor prognosis in different cancer types [48]. This study deeply investigated the role of pyroptosis in GC pathogenesis and the correlation between *ELANE* and GC prognosis prediction.

The enrichment analyses were conducted to determine the function of *ELANE*. Multivariate Cox analysis results indicated that age, M stage, and *ELANE* expression were independent risk factors for GC (Fig. 5B). Subsequently, a nomogram incorporating age, M stage, and *ELANE* genes (Fig. 5C) was applied to predict the survival rates of GC cases. According to the relevant calibration curve results, it can be found that the nomogram significantly predicted 1- and 3-year survival rates (Fig. 5D). We found that *ELANE* is associated with poor clinical prognosis. Regarding the mechanisms underlying the function of *ELANE* in the occurrence and progression of GC, the main findings of GO and KEGG analyses are associated with processes such as "membrane potential regulation," "human immunity," "transmembrane transporter complex," "transporter complex," and "ion channel activity". Many of these overlap with the pyroptosis process, indicating that *ELANE* may participate in the pathological process of GC by impacting the pyroptosis process through the above channels. Particularly, *ELANE* was mainly enriched in hsa04024 (cAMP signaling pathway) (Fig. 6). According to previous reports, activating the cAMP/PKA pathway induces pyroptosis in breast cancer cells [49], which may also affect the cAMP/PKA signaling pathway in GC. By Gene Set Enrichment Analysis (Fig. 7), we found *ELANE* could influence the pathway of ADORA2B mediated anti-inflammatory cytokines production. ADORA2B, one of four purine nucleoside adenosine (ADO) sensing receptors [50], is closely associated with inflammation [51,52] and many common tumors, such as glioblastoma, pancreatic cancer, and so on [53–56]. In cancer, it plays important roles in proliferation, apoptosis, angiogenesis, metastasis, and immunomodulation [57]. Some evidence suggests that the adenosine receptor is intricately tied to the mitogen-activated protein kinase (MAPK) signaling pathway [58]. Previous studies have suggested that the MAPK signaling pathway could inhibit pyroptosis [59,60]. Thus, we speculated that *ELANE* might interact with ADORA2B and mediate the pyroptosis of GC via the MAPK signaling pathway.

Fig. 8A and B shows that *ERBB2* interacted closely with other key genes, followed by *NKX2-1*. *ERBB2* is human epidermal growth factor receptor-2, also known as *HER2*. It is involved in the occurrence and metastasis of various tumors, including GC, and is a well-known immunotherapeutic target [61]. *NKX2-1*, a transcription factor containing homeoboxes named TTF-1, functions as a "lineage survival" cancer-related gene in lung adenocarcinoma [62]. Although increasing evidence supports the carcinogenic effect of *NKX2-1*, its expression also exhibits a clinical effect in inhibiting tumor progression [63]. *ELANE* is closely related to these two genes, suggesting that *ERBB2*, *NKX2-1,* and *ELANE* may be important factors in the pathological process of GC, providing further insights into the role of *ELANE* in GC immunotherapy. However, it remains unclear in recent research whether these genes are involved in pyroptosis in GC. *ELANE* may be a "door" to initiate exploration in this area. In addition, we found that *hsa-mir-126-3p*, *hsa-mir-146a-5p*, and *hsa-mir-31-5p* regulate *ELANE* (Fig. 8C). Among them, *hsa-mir-126-3p* and *hsa-mir-146a-5p* are associated with GC but not with pyroptosis [64], according to the literature. Therefore, they may affect the molecular mechanism of GC by regulating *ELANE*. Furthermore, the TF-*ELANE* network consisted of 23 nodes and 22 interaction relationship pairs (Fig. 8D), indicating a degree of interaction between TFs and *ELANE* in GC. These TFs may participate in GC via the TF-*ELANE* pathway. Moreover, for the first time, we identified *ELANE* as a target of 10 drugs. This provides predictions for the development of *ELANE* target drugs, which is beneficial for the development of GC target drugs (Fig. 8E). As the immune system plays a crucial role in tumor evolution and immune infiltration is closely related to immunotherapy responsiveness, we performed an immune infiltration analysis to investigate the differences in immune cell infiltration between two groups of patients with GC. We found that the *ELANE* level was positively related to B cells, $CD4^+$ T cells, and macrophages and negatively related to tumor purity (Fig. 9A). Additionally, we calculated the immune cell infiltration based on the CIBERSORT method. Overall, 10 immune cell types in the TCGA dataset exhibited obvious differences between the low and high-*ELANE* groups (Fig. 9C). These findings suggest that *ELANE* is a potential therapeutic target in anti-tumor immunity. The key point of this paper is that we first proved the high expression of *ELANE* in tumor samples of clinical patients with GC and verified the existence of a pyroptosis process linked to high *ELANE* levels in GC tumor cells through cell experiments (Fig. 10).

Based on the above research results, we could infer that *ELANE* is not only a potential biomarker in the diagnosis and prognosis of GC but also a key target for immunotherapy. This provides theoretical support for the mechanism in which *ELANE* regulates the pathological process of GC by affecting the pyroptosis process of GC cells, thus facilitating further research and development of anti-*ELANE* tumor drugs.

However, this study had some limitations. Firstly, our study did not further verify how *ELANE* regulates the pyroptosis process of GC. Next, we will perform in vivo and in vitro experiments to verify the mechanism of action of *ELANE*. Secondly, the patient's clinical information was obtained from the TCGA database; we will collect real-world patient information from our hospital. Finally, drawing conclusions about miRNAs and drug effects lacked inadequate experimental validation; therefore, the prediction results should be

verified by subsequent experiments to confirm their biological function and clinical application value.

5. Conclusion

ELANE has a higher level in GC tissues, and high *ELANE* expression is related to poor survival and prognosis of patients with GC. *ELANE* participates in pyroptosis and immune infiltration in GC. Therefore, it is a promising prognostic biomarker for pyroptosis in GC.

Ethics approval and consent to participate

Not applicable.

Data availability statement

All data are fully available without restriction. Additional information is available from the corresponding authors upon request.

CRediT authorship contribution statement

Ming Cui: Writing – original draft, Visualization, Validation, Methodology, Investigation, Formal analysis, Data curation. **Xiaowu Wang:** Writing – original draft, Visualization, Validation, Software, Methodology, Investigation, Formal analysis, Data curation. **Haiyan Qiao:** Visualization, Validation, Software, Formal analysis, Data curation. **Shixi Wu:** Writing – review & editing, Supervision, Project administration, Conceptualization. **Bingbing Shang:** Writing – review & editing, Supervision, Resources, Project administration, Funding acquisition, Conceptualization.

Declaration of competing interest

The authors declare the following financial interests/personal relationships which may be considered as potential competing interests:Bingbing Shang reports financial support was provided by Dalian Peak Plan. If there are other authors, they declare that they have no known competing financial interests or personal relationships that could have appeared to influence the work reported in this paper.

Acknowledgments

We thank Editage (www.editage.cn) for the linguistic editing of the manuscript.

Appendix A. Supplementary data

Supplementary data to this article can be found online at https://doi.org/10.1016/j.heliyon.2024.e34360.

References

[1] E.C. Smyth, M. Nilsson, H.I. Grabsch, N.C. van Grieken, F. Lordick, Gastric cancer, Lancet 396 (10251) (2020) 635–648.
[2] J.Y. Tuo, J.H. Bi, H.Y. Yuan, Y.F. Jiang, X.W. Ji, H.L. Li, Y.B. Xiang, Trends of stomach cancer survival: a systematic review of survival rates from population-based cancer registration, J. Dig. Dis. 23 (1) (2022) 22–32.
[3] M. Banks, D. Graham, M. Jansen, T. Gotoda, S. Coda, M. di Pietro, N. Uedo, P. Bhandari, D.M. Pritchard, E.J. Kuipers, et al., British Society of Gastroenterology guidelines on the diagnosis and management of patients at risk of gastric adenocarcinoma, Gut 68 (9) (2019) 1545–1575.
[4] R.A. de Mello, G.A. Amaral, N.M. Neves, E.G. Lippo, F. Parini, S. Xu, M. Tolia, N. Charalampakis, H. Tadokoro, P. Castelo-Branco, J. Zhu, Current and potential biomarkers in gastric cancer: a critical review of the literature, Future Oncol. 17 (25) (2021 Sep) 3383–3396.
[5] J.Y. Zhong, H.B. Chen, D.Z. Ye, Z.J. Deng, J.J. Shao, J.W. Han, J.H. Yuan, N.Y. Deng, Molecular mechanism of Ganoderma against gastric cancer based on network pharmacology and experimental test, Zhongguo Zhongyao Zazhi 47 (1) (2022 Jan) 203–223 (Chinese).
[6] M. Sasahara, M. Kanda, Y. Kodera, Update on molecular biomarkers for diagnosis and prediction of prognosis and treatment responses in gastric cancer, Histol. Histopathol. 36 (8) (2021) 817–832.
[7] X. Ju, Z. Yang, H. Zhang, Q. Wang, Role of pyroptosis in cancer cells and clinical applications, Biochimie 185 (2021) 78–86.
[8] Y. Tan, Q. Chen, X. Li, Z. Zeng, W. Xiong, G. Li, X. Li, J. Yang, B. Xiang, M. Yi, Pyroptosis: a new paradigm of cell death for fighting against cancer, J. Exp. Clin. Cancer Res. 40 (1) (2021 May 3) 153.
[9] X. Liang, Y. Qin, D. Wu, Q. Wang, H. Wu, Pyroptosis: a double-edged sword in lung cancer and other respiratory diseases, Cell Commun. Signal. 22 (1) (2024 Jan 15) 40.
[10] X. Xia, X. Wang, Z. Cheng, et al., The role of pyroptosis in cancer: pro-cancer or pro-"host"? Cell Death Dis. 10 (9) (2019) 650.
[11] W. Zhou, H. Liu, Z. Yuan, J. Zundell, M. Towers, J. Lin, S. Lombardi, H. Nie, B. Murphy, T. Yang, C. Wang, L. Liao, A.R. Goldman, T. Kannan, A.V. Kossenkov, R. Drapkin, L.J. Montaner, D.T. Claiborne, N. Zhang, S. Wu, R. Zhang, Targeting the mevalonate pathway suppresses ARID1A-inactivated cancers by promoting pyroptosis, Cancer Cell 41 (4) (2023 Apr 10) 740–756.e10.
[12] Z. Wang, Z. Dai, H. Zhang, N. Zhang, X. Liang, L. Peng, J. Zhang, Z. Liu, Y. Peng, Q. Cheng, Z. Liu, Comprehensive analysis of pyroptosis-related gene signatures for glioblastoma immune microenvironment and target therapy, Cell Prolif. 56 (3) (2023 Mar) e13376.
[13] B. Zhang, Z. Li, K. Wang, M. Duan, Y. Yin, Q. Zhan, F. Wang, R. An, Exploration of pyroptosis-associated prognostic gene signature and lncRNA regulatory network in ovarian cancer, Comput. Biol. Med. 164 (2023) 107343.

[14] M. Liu, Q. Li, Y. Liang, Pyroptosis-related genes prognostic model for predicting targeted therapy and immunotherapy response in soft tissue sarcoma, Front. Pharmacol. 14 (2023 May 5) 1188473.
[15] W. Zeng, G.A. Silverman, Remold-O'Donnell E: structure and sequence of human M/NEI (monocyte/neutrophil elastase inhibitor), an Ov-serpin family gene, Gene 213 (1–2) (1998) 179–187.
[16] Z. Shu, X.H. Li, X.M. Bai, Z.Y. Zhang, L.P. Jiang, X.M. Tang, X.D. Zhao, Clinical characteristics of severe congenital neutropenia caused by novel ELANE gene mutations, Pediatr. Infect. Dis. J. 34 (2) (2015) 203–207.
[17] S. Novovic, A.M. Andersen, M. Nord, M. Astrand, T. Ottosson, L.N. Jørgensen, M.B. Hansen, Activity of neutrophil elastase reflects the progression of acute pancreatitis, Scand. J. Clin. Lab. Invest. 73 (6) (2013) 485–493.
[18] B. Peng, J. Hu, X. Fu, ELANE: an emerging lane to selective anticancer therapy, Signal Transduct. Targeted Ther. 6 (1) (2021 Oct 1) 358.
[19] S. Song, Y. Zhao, T. Fu, Y. Fan, J. Tang, X. Wang, C. Liu, X. Chen, ELANE promotes M2 macrophage polarization by down-regulating PTEN and participates in the lung cancer progression, Immunol. Invest. 52 (1) (2023) 20–34.
[20] Z. Wei, B. Wu, L. Wang, J. Zhang, A large-scale transcriptome analysis identified ELANE and PRTN3 as novel methylation prognostic signatures for clear cell renal cell carcinoma, J. Cell. Physiol. 235 (3) (2020) 2582–2589.
[21] X. Zhang, Q. Yang, A pyroptosis-related gene panel in prognosis prediction and immune microenvironment of human endometrial cancer, Front. Cell Dev. Biol. 9 (2021 Oct 14) 705828.
[22] Z. Qu, Y. Han, Q. Zhu, W. Ding, Y. Wang, Y. Zhang, W. Wei, Y. Lei, M. Li, Y. Jiao, et al., A novel neutrophil extracellular traps signature for overall survival prediction and tumor microenvironment identification in gastric cancer, J. Inflamm. Res. 16 (2023) 3419–3436.
[23] S.F. Kadasah, Establishment and systematic evaluation of gastric cancer classification model based on pyroptosis, Diagnostics 12 (11) (2022 Nov 18) 2858.
[24] S. Davis, P.S. Meltzer, GEOquery: a bridge between the gene expression Omnibus (GEO) and BioConductor, Bioinformatics 23 (14) (2007) 1846–1847.
[25] A. Colaprico, T.C. Silva, C. Olsen, L. Garofano, C. Cava, D. Garolini, T.S. Sabedot, T.M. Malta, S.M. Pagnotta, I. Castiglioni, et al., TCGAbiolinks: an R/Bioconductor package for integrative analysis of TCGA data, Nucleic Acids Res. 44 (8) (2016) e71.
[26] M.E. Ritchie, B. Phipson, D. Wu, Y. Hu, C.W. Law, W. Shi, G.K. Smyth, Limma powers differential expression analyses for RNA-sequencing and microarray studies, Nucleic Acids Res. 43 (7) (2015) e47.
[27] M.I. Love, W. Huber, S. Anders, Moderated estimation of fold change and dispersion for RNA-seq data with DESeq2, Genome Biol. 15 (12) (2014) 550.
[28] Z. Gu, R. Eils, M. Schlesner, Complex heatmaps reveal patterns and correlations in multidimensional genomic data, Bioinformatics 32 (18) (2016) 2847–2849.
[29] G. Yu, L.G. Wang, Y. Han, Q.Y. He, clusterProfiler: an R package for comparing biological themes among gene clusters, OMICS 16 (5) (2012) 284–287.
[30] A. Subramanian, P. Tamayo, V.K. Mootha, S. Mukherjee, B.L. Ebert, M.A. Gillette, A. Paulovich, S.L. Pomeroy, T.R. Golub, E.S. Lander, et al., Gene set enrichment analysis: a knowledge-based approach for interpreting genome-wide expression profiles, Proc. Natl. Acad. Sci. U. S. A. 102 (43) (2005) 15545–15550.
[31] G. Yu, Gene ontology semantic similarity analysis using GOSemSim, Methods Mol. Biol. 2117 (2020) 207–215.
[32] D. Szklarczyk, A.L. Gable, D. Lyon, A. Junge, S. Wyder, J. Huerta-Cepas, M. Simonovic, N.T. Doncheva, J.H. Morris, P. Bork, L.J. Jensen, C.V. Mering, STRING v11: protein-protein association networks with increased coverage, supporting functional discovery in genome-wide experimental datasets, Nucleic Acids Res. 47 (D1) (2019 Jan 8) D607–D613.
[33] J. Xia, M.J. Benner, R.E. Hancock, NetworkAnalyst-integrative approaches for protein-protein interaction network analysis and visual exploration, Nucleic Acids Res. 42 (2014) W167–W174.
[34] ENCODE Project Consortium, An integrated encyclopedia of DNA elements in the human genome, Nature 489 (7414) (2012) 57–74.
[35] J. Ru, P. Li, J. Wang, W. Zhou, B. Li, C. Huang, P. Li, Z. Guo, W. Tao, Y. Yang, et al., TCMSP: a database of systems pharmacology for drug discovery from herbal medicines, J. Cheminf. 6 (2014) 13.
[36] X. Robin, N. Turck, A. Hainard, N. Tiberti, F. Lisacek, J.C. Sanchez, M. Müller, pROC: an open-source package for R and S+ to analyze and compare ROC curves, BMC Bioinf. 12 (2011) 77.
[37] J. Liu, T. Lichtenberg, K.A. Hoadley, L.M. Poisson, A.J. Lazar, A.D. Cherniack, A.J. Kovatich, C.C. Benz, D.A. Levine, A.V. Lee, et al., An integrated TCGA pan-cancer clinical data Resource to drive high-quality survival outcome analytics, Cell 173 (2) (2018) 400–416.e411.
[38] A.M. Newman, C.B. Steen, C.L. Liu, A.J. Gentles, A.A. Chaudhuri, F. Scherer, M.S. Khodadoust, M.S. Esfahani, B.A. Luca, D. Steiner, et al., Determining cell type abundance and expression from bulk tissues with digital cytometry, Nat. Biotechnol. 37 (7) (2019) 773–782.
[39] L.C. Wang, Y.L. Wang, B. He, Y.J. Zheng, H.C. Yu, Z.Y. Liu, R.R. Fan, X. Zan, R.C. Liang, Z.P. Wu, X. Tang, G.Q. Wang, J.G. Xu, L.X. Zhou, Expression and clinical significance of VISTA, B7-H3, and PD-L1 in glioma, Clin. Immunol. 245 (2022 Dec) 109178.
[40] B. Shang, R. Wang, H. Qiao, X. Zhao, L. Wang, S. Sui, Multi-omics analysis of pyroptosis regulation patterns and characterization of tumor microenvironment in patients with hepatocellular carcinoma, PeerJ 11 (2023 May 11) e15340.
[41] Z. Rao, Y. Zhu, P. Yang, Z. Chen, Y. Xia, C. Qiao, W. Liu, H. Deng, J. Li, P. Ning, et al., Pyroptosis in inflammatory diseases and cancer, Theranostics 12 (9) (2022) 4310–4329.
[42] Y. Fang, S. Tian, Y. Pan, W. Li, Q. Wang, Y. Tang, T. Yu, X. Wu, Y. Shi, P. Ma, Y. Shu, Pyroptosis: a new frontier in cancer, Biomed. Pharmacother. 121 (2020 Jan) 109595.
[43] L.M. Coussens, Z. Werb, Inflammation and cancer, Nature 420 (6917) (2002) 860–867.
[44] W. Jia, Q. Luo, J. Wu, Y. Shi, Q. Guan, Neutrophil elastase as a potential biomarker related to the prognosis of gastric cancer and immune cell infiltration in the tumor immune microenvironment, Sci. Rep. 13 (1) (2023 Aug 18) 13447.
[45] C. Cui, K. Chakraborty, X.A. Tang, G. Zhou, K.Q. Schoenfelt, K.M. Becker, A. Hoffman, Y.F. Chang, A. Blank, C.A. Reardon, H.A. Kenny, T. Vaisar, E. Lengyel, G. Greene, L. Becker, Neutrophil elastase selectively kills cancer cells and attenuates tumorigenesis, Cell 184 (12) (2021 Jun 10) 3163–3177.e21.
[46] S. Kesavardhana, R.K.S. Malireddi, T.D. Kanneganti, Caspases in cell death, inflammation, and pyroptosis, Annu. Rev. Immunol. 38 (2020) 567–595.
[47] R. Yang, L. Zhong, X.Q. Yang, K.L. Jiang, L. Li, H. Song, B.Z. Liu, Neutrophil elastase enhances the proliferation and decreases apoptosis of leukemia cells via activation of PI3K/Akt signaling, Mol. Med. Rep. 13 (5) (2016) 4175–4182.
[48] X. Chu, Z. Sun, D.S. Baek, W. Li, J.W. Mellors, S.D. Shapiro, D.S. Dimitrov, Human antibody domains and fragments targeting neutrophil elastase as candidate therapeutics for cancer and inflammation-related diseases, Int. J. Mol. Sci. 22 (20) (2021 Oct 15) 11136.
[49] C. Chen, S. Yuan, X. Chen, J. Xie, Z. Wei, Xihuang pill induces pyroptosis and inhibits progression of breast cancer cells via activating the cAMP/PKA signalling pathway, Am. J. Cancer Res. 13 (4) (2023) 1347–1362.
[50] E.A. Vecchio, P.J. White, L.T. May, The adenosine A(2B) G protein-coupled receptor: recent advances and therapeutic implications, Pharmacol. Therapeut. 198 (2019) 20–33.
[51] X. Yuan, T. Mills, M.F. Doursout, S.E. Evans, M.F. Vidal Melo, H.K. Eltzschig, Alternative adenosine Receptor activation: the netrin-Adora2b link, Front. Pharmacol. 13 (2022 Jul 15) 944994.
[52] K.-C. Ngamsri, F. Fabian, A. Fuhr, J. Gamper-Tsigaras, A. Straub, D. Fecher, M. Steinke, H. Walles, J. Reutershan, F.M. Konrad, Sevoflurane exerts protective effects in murine peritonitis-induced sepsis via hypoxia-inducible factor 1α/adenosine A2B receptor signaling, Anesthesiology 135 (1) (2021) 136–150.
[53] V. Bova, A. Filippone, G. Casili, M. Lanza, M. Campolo, A.P. Capra, A. Repici, L. Crupi, G. Motta, C. Colarossi, G. Chisari, S. Cuzzocrea, E. Esposito, I. Paterniti, Adenosine targeting as a new strategy to decrease glioblastoma aggressiveness, Cancers 14 (16) (2022 Aug 20) 4032.
[54] L.N. Strickland, E.Y. Faraoni, W. Ruan, X. Yuan, H.K. Eltzschig, J.M. Bailey-Lundberg, The resurgence of the Adora2b receptor as an immunotherapeutic target in pancreatic cancer, Front. Immunol. 14 (2023 Apr 28) 1163585.
[55] M. Wilkat, H. Bast, R. Drees, J. Dünser, A. Mahr, N. Azoitei, R. Marienfeld, F. Frank, M. Brhel, A. Ushmorov, et al., Adenosine receptor 2B activity promotes autonomous growth, migration as well as vascularization of head and neck squamous cell carcinoma cells, Int. J. Cancer 147 (1) (2020) 202–217.
[56] J. Liao, D.N. Zeng, J.Z. Li, Q.M. Hua, Z. Xiao, C. He, K. Mao, L.Y. Zhu, Y. Chu, W.P. Wen, et al., Targeting adenosinergic pathway enhances the anti-tumor efficacy of sorafenib in hepatocellular carcinoma, Hepatol. Int. 14 (1) (2020) 80–95.
[57] Z.G. Gao, M. Haddad, K.A. Jacobson, A2B adenosine receptor signaling and regulation, Purinergic Signalling (2024) 1–20.

[58] H. Yang, Z. Zhang, K. Zhao, Y. Zhang, X. Yin, G. Zhu, Z. Wang, X. Yan, X. Li, T. He, K. Wang, Targeting the adenosine signaling pathway in macrophages for cancer immunotherapy, Hum. Immunol. 85 (3) (2024 May) 110774.
[59] Z. Liu, X. Yao, W. Jiang, W. Li, S. Zhu, C. Liao, L. Zou, R. Ding, J. Chen, Advanced oxidation protein products induce microglia-mediated neuroinflammation via MAPKs-NF-κB signaling pathway and pyroptosis after secondary spinal cord injury, J. Neuroinflammation 17 (1) (2020 Mar 20) 90.
[60] R. Zhou, X. Yang, X. Li, Y. Qu, Q. Huang, X. Sun, D. Mu, Recombinant CC16 inhibits NLRP3/caspase-1-induced pyroptosis through p38 MAPK and ERK signaling pathways in the brain of a neonatal rat model with sepsis, J. Neuroinflammation 16 (1) (2019 Nov 27) 239.
[61] M.M. Moasser, The oncogene HER2: its signaling and transforming functions and its role in human cancer pathogenesis, Oncogene 26 (45) (2007) 6469–6487.
[62] G. Mollaoglu, A. Jones, S.J. Wait, A. Mukhopadhyay, S. Jeong, R. Arya, S.A. Camolotto, T.L. Mosbruger, C.J. Stubben, C.J. Conley, et al., The lineage-defining transcription factors SOX2 and NKX2-1 determine lung cancer cell fate and shape the tumor immune microenvironment, Immunity 49 (4) (2018) 764–779.e769.
[63] T. Yamaguchi, Y. Hosono, K. Yanagisawa, T. Takahashi, NKX2-1/TTF-1: an enigmatic oncogene that functions as a double-edged sword for cancer cell survival and progression, Cancer Cell 23 (6) (2013) 718–723.
[64] I.K. Stefanou, N. Dovrolis, M. Gazouli, D. Theodorou, G.K. Zografos, K.G. Toutouzas, miRNAs expression pattern and machine learning models elucidate risk for gastric GIST, Cancer Biomarkers 33 (2) (2022) 237–247.